

The reason of cracking in bottom gallery of SefidRud Buttress Dam and earthquake and post earthquake performance

Hasan Mirzabozorg^{*1}, Mohsen Ghaemian² and Amirhossein Roohezamin¹

¹Department of Civil Engineering, K. N. Toosi University of Technology, Valiasr Avenue, Tehran, Iran

²Department of Civil Engineering, Sharif University of Technology; Azadi Avenue,
P.O. Box 11365-9313, Tehran, Iran

(Received January 19, 2019, Revised April 3, 2019, Accepted April 17, 2019)

Abstract. Present study concerns the safety evaluation of SefidRud dam's block No. 18 regarding probable crack propagation in the foundation gallery under a MCE record. Accordingly, a 3D finite element model of the block in companion with the reservoir and the foundation is modeled. All the associated thermal and structural parameters are derived via calibration with the records of thermometers and pendulums installed inside the dam body. The origination of the cracks and their whereabouts are determined by primary thermal and static analyses and through a linear dynamic analysis the potential failure zone and their extent and level are studied. The foundation gallery is the most probable zone among the other intensive tensile stress area to compromise the dam stability. Therefore, the nonlinear analysis of this risky region is inevitable. The results depict the permissible expansion of the cracks inside the gallery even under another future earthquake in MCE level. As a consequence, the general dam performance is assessed safe in spite of the seepage flow rate growth from the gallery fractures.

Keywords: Buttress dam; calibration; cracked Initial condition; post earthquake stability; SefidRud dam

1. Introduction

On June 20, 1990 Manjil-Rudbar earthquake occurred with the magnitude of 7.4 in Richter scale and devastated some densely populated areas in north and north-west provinces of Iran, namely Gilan and Zanjan. Beside the heavy mortality and damages of rural and urban infrastructures and facilities, induced cracks of SefidRud concrete buttress dam and its probable failure was a matter of some concern. This 106 m dam which consists of 30 blocks was constructed across Ghezel-Uzan and Shah-Roud rivers in the vicinity of Mangil City in Gilan Province and was distanced just 10 km from epicenter of the earthquake (Ahmadi and Khoshrang 1992). As a consequence, substantial damages and overall cracks occurred from upstream through downstream face near slopping transition and in construction joints in almost all the blocks, except block No.5 (Ghaemmaghani and Ghaemian 2010). This damage and the one formed on the downstream face of the buttresses are the damage patterns expected in buttress dams like Hsinfengkiang Dam in China suffering a crack in downstream kink (Shen *et al.* 1974) or the

*Corresponding author, Associate Professor, E-mail: mirzabozorg@kntu.ac.ir

anticipated crack in Grua Raului dam in Romania (Ilinca *et al.* 2014). Back to the SefidRud dam case, the central blocks were highly affected by the damages; for instance, in block No.15 a wedge was formed on the downstream face which was displaced about 20mm toward downstream and caused substantial leakage (Ahmadi *et al.* 1992, Ghaemmaghani and Ghaemian 2010). In spite of the seemingly destructive damages (especially in central blocks), the total stability of the dam body was preserved. This subject was analyzed and observed numerically (Ahmadi *et al.* 1992, Ghaemian 1996, Ghaemian and Ghobarah 1997, 1999) and experimentally (Ghaemmaghani and Ghaemian 2008). However, owing to the excessive leakage and probable failure as a consequence of the future earthquake, the rehabilitation operation was inevitable. This operation included resin grouting and installing post stressed cables (Arcangeli and Ciabbari 1994) which was initiated 5 months after the earthquake. The rehabilitation functionality was assessed experimentally on a shaking table where the retrofitted dam could endure the peak ground acceleration 22% higher than the one causing the damages at the first place (Ghaemmaghani and Ghaemian 2010).

Most of the previous researches were focused on safety analysis of block No.15 which was the most demolished block during Manjil earthquake. Nevertheless, propagation of the formed crack in the foundation gallery which has existed since the construction phase and the safe performance of the dam, which may be compromised by that is of less investigated and yet vital issue. After the 1990s earthquake, the seepage from mentioned crack substantially exceeded; therefore, stability analysis of SefidRud dam regarding the extension and propagation of such cracks was of high priority which was inspected by Yekom consulting engineers, (Yekom Consulting Engineers 2007), but just under the static loads while the seismic performance has not yet been paid attention.

The present study comprises the seismic safety analysis of SefidRud dam's block No.18 in regard to the crack existence in the foundation gallery. For this purpose, a comprehensive 3-D finite element model of block No.18 including the outlet, the gallery, and the post stressed cables in companion with the foundation and the reservoir is provided. Initially, to determine the decent and precise thermal and mechanical parameters, primary thermal and structural analyses are executed and the associated responses are calibrated with the data gathered from thermometers and the direct pendulums installed inside the dam body. The stability investigation is proceeded by a linear dynamic analysis under ABBAR station recorded earthquake as a MCE record to detect the potential region of failure and then, based on the gravity dams DCR curve, a nonlinear seismic analysis of vulnerable regions is conducted to assess the seismic performance of the block. At last, the static and dynamic post-earthquake behaviors of the structure are investigated thoroughly.

2. Structural finite element model

As mentioned before, the buttress No.18 is modeled and analyzed in finite element based software, which is capable of carrying out linear and nonlinear seismic analyses considering dam-reservoir interaction. The dam body model includes all the geometric and technical specifications such as post-stressed cables, the bottom outlet and the bottom gallery (see Fig. 1). These specifications are elaborated in Table 1 along with the element types utilized for each part of the provided model. Also, Fig. 2 schematically depicts the overall finite element model of the buttress No.18.

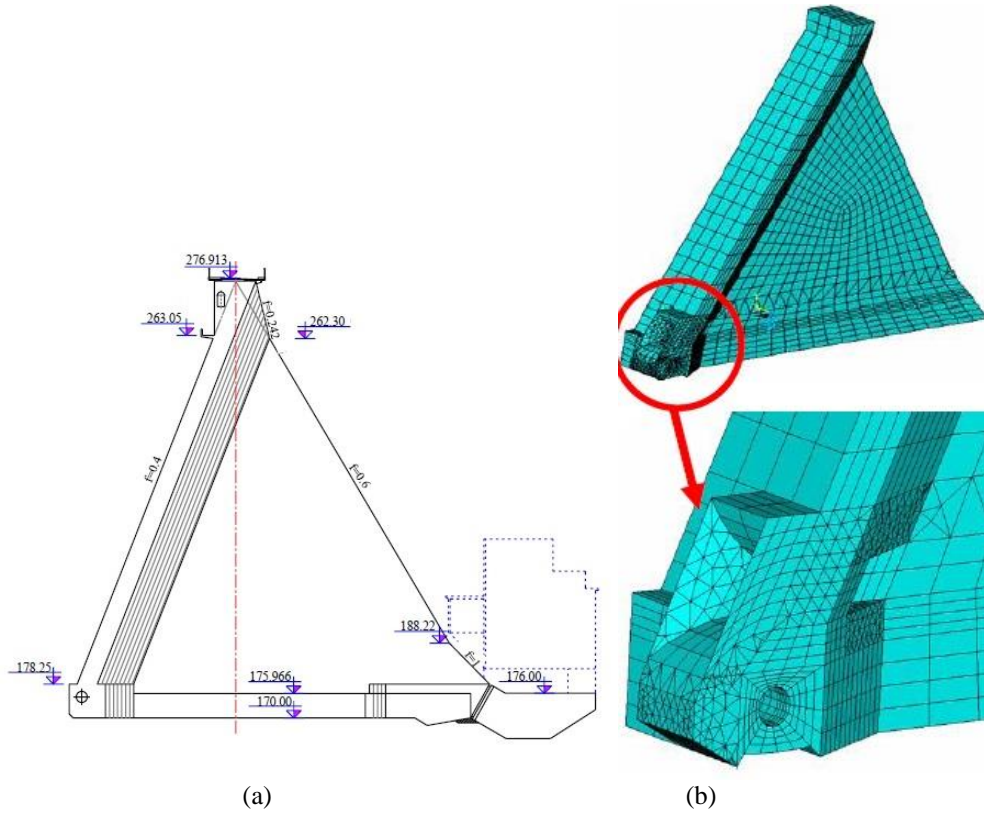


Fig. 1 Buttress No. 18; (a) geometric Specifications and (b) meshing including the bottom outlet and the gallery

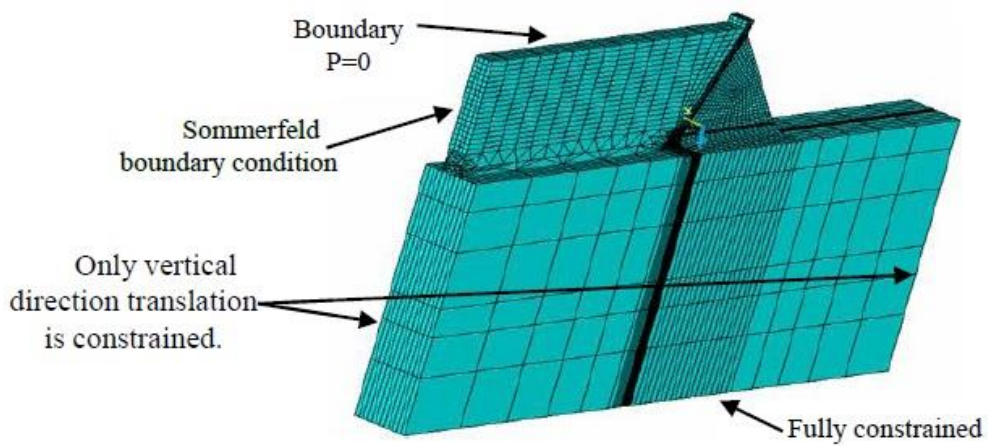


Fig. 2 The finite element model of buttress No.18 system

Table 1 Element types of the dam system components and geometrical specification

Part of the dam system	Element type	Geometrical specification
Dam body	SOLID*	96m height- U/S slope: 1 to 0.4- D/S slope: 1 to 0.6- Crest width:10.5 m
Foundation	SOLID*	Length, depth and width of about 1.5 times the dam height
Reservoir	FLUID**	Length of 240 m (2.5 times the dam height) with constant section
Post stressed cables	LINK***	12 anchors of 8.4MN working load, inclined between 6.5 and 21.5° in planes perpendicular to the dam axis (Ghaemmaghami and Ghaemian 2010)
Bottom outlet/Gallery	SOLID****	

*8-node element with 3 translational DOFs in each node

** 8-node element with 3 translational DOFs and one pressure DOF in each node

*** 2-node element with 3 translational DOFs in each node.

**** 20-node element with 3 translational DOFs in each node

To model the interaction between the dam body and the reservoir, the coupled structure-reservoir dynamic equations are solved simultaneously (Ghaemian and Ghobarah 1998). The reservoir free surface is modeled by considering its pressure equals to zero. Moreover, the *Sommerfeld* equation is assigned to the reservoir truncated boundary condition at the distance designated in Table 1. Regarding the massless foundation assumption, the nodes at the foundation bottom are fully constrained while the nodes at its far end are constrained only in vertical direction.

3. Parameters calibration

In analysis of a model, one can find promising and precise results, which have an acceptable agreement with the extracted records from the real case if the associated parameters and specifications are chosen based on valid sources. In the analysis of a dam, beside the reports and the related papers, calibration of the responses with controlling apparatuses records makes it possible to have qualified and validated outcomes. As a result, in the following case study in regard to their contribution in the crack extension, thermal and structural calibrations are anticipated.

3.1 Thermal calibration

A transient thermal model is applied for the calibration case during the time interval of year 1996 to year 2000 when the results deemed to be stable. The necessary thermal parameters to model the concrete in the numerical model are provided in Table 2. It is worthy to note that time dependent thermal distribution is not applied for the foundation, but of annual mean is considered for it.

Table 2 Material thermal specifications applied in numerical model

Property	Concrete	Foundation
Specific heat J/(kg °C)	870-1080 (921.1)*	-
Thermal conductivity (J/m/ °C/hr)	8373.6	-
Convection coefficient (J/ m ² / °C/hr)	55692**	-

*Values used in numerical model.

** For average annual wind speed of 2.5 m/s

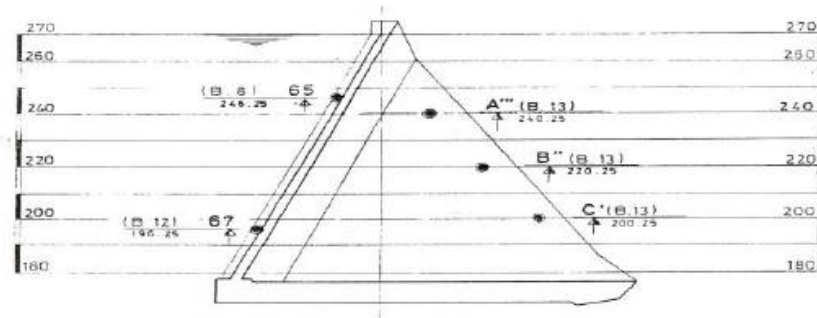


Fig. 3 The approximate location of the thermometers in buttress No.13 (the rest of the thermometers are reported defected)

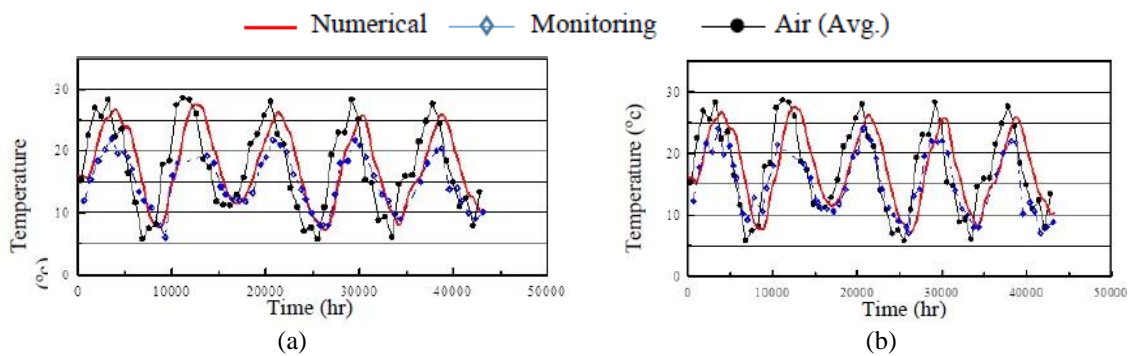


Fig. 4 Comparison of the thermal analysis results with the records obtained from thermometers (a) A3, and (b)

The monthly mean temperature is considered as the circumstance temperature and for the temperature distribution along the reservoir depth, Bofang empirical-analytical relation (Bofang 1997) is utilized. Comparing the thermal analysis results with records of thermometers A3 and C1 installed in buttress No.13 at elevations of 240.25 m and 200.25 m (Fig. 3), respectively, for the time duration of year 1996 to year 2000 and considering the approximation emanated from data generalization to buttress No.18, the adequate functionality of the applied model and parameters can be concluded (see Fig. 4).

Table 3 Considered time for finite element model and structural calibration

No.	Date	Description
1	March, 29, 1998	Base Time
2	April, 4, 1999	The maximum displacement toward downstream relative to the base time in year 1999
3	Aug, 8, 1999	The maximum displacement toward upstream relative to the base time in year 1999
4	April, 3, 2000	The maximum displacement toward downstream relative to the base time in year 2000
5	Aug, 13, 2000	The maximum displacement toward upstream relative to the base time in year 2000
6	March, 11, 2001	The maximum displacement toward downstream relative to the base time in year 2001

3.2 Structural calibration

The upstream-downstream displacement is considered as the calibration criterion and the one calculated from the finite element model is calibrated with the one extracted from direct pendulums installed on buttress No.18. The calibration analysis is limited to the dates specified in Table 3.

In calibration analyses, the imposed loads are limited to the self-weight, hydrostatic and thermal loads because of the fading of the nonlinear effects emanated from concrete creep and foundation joints after the earthquake and origination of the displacement from water level and temperature fluctuation. The structural parameters being verified through the calibration are listed in Table 4.

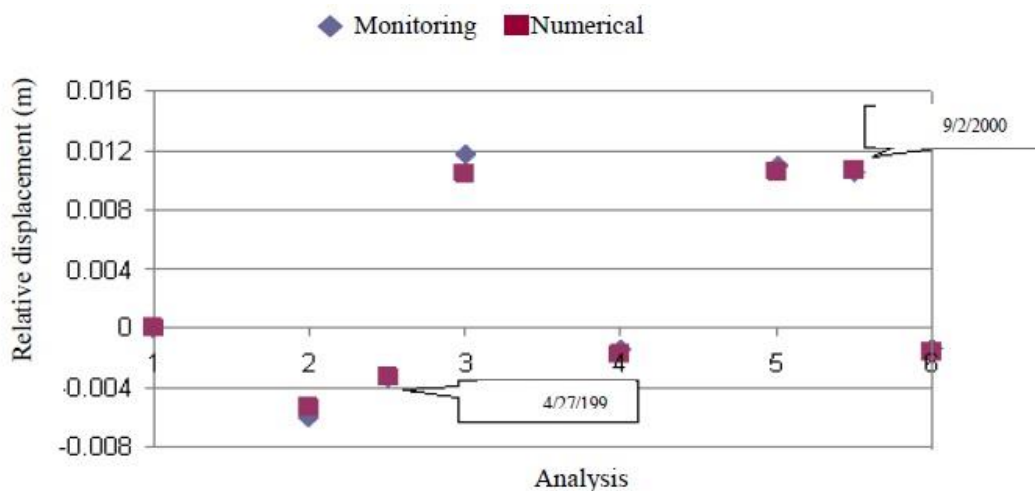


Fig. 5 Comparison between structural analysis and the upstream-downstream pendulum of buttress No.18

Table 4 Applied structural parameters in model

Parameters	Values,(Yekom Consulting Engineers 2007)
Concrete density (kg/m ³)	2230
Concrete elasticity modulus (GPa)	19
Concrete Poisson's ratio	0.15
Concrete thermal expansion coefficient (1/°C)	12E-6
Concrete reference temperature (°C)	13
Concrete elasticity modulus for thermal loading (creep affection) (GPa)	0.7*19*
Concrete tensile strength (MPa)	2.15
Concrete apparent tensile strength (MPa)	2.9
Foundation** deformation modulus (GPa)	5
Foundation Poisson's ratio	0.22
Water density (kg/m ³)	1000
Wave velocity in water (m/s)	1438
Wave absorption coefficient	0.8***

* The creep affection is only considered in thermal analysis by decreasing of the concrete modulus of elasticity

** The foundation is considered "massless", so the rock density is not required

*** Referring to FERC document (FERC, 1999)

Comparing the calculated results with the measured upstream-downstream displacements is shown in Fig. 5 for the specified dates (see Table 3) plus two more dates which are corresponding to the maximum and minimum reservoir water levels. Regarding the numerical and monitoring results coincident in Fig. 5 along with the results from the previous studies, normal values in similar dams and engineering references, it could be claimed that the parameters in Table 4 has an adequate accuracy for future analyses in spite of adequate data deprivation to express an accurate view. It is worth mentioning that varying parameters during the structural calibration process are concrete elasticity modulus, concrete thermal expansion coefficient, creep affection and foundation deformation modulus.

4. Linear dynamic analysis

The aim of linear dynamic analysis in the current study is predicting the candidate areas for cracking within the dam body. The dynamic analysis is restricted to two critical dates of April, 4, 1999 (water level 266 m) and Aug, 8, 1999 (water level 225 m) which are corresponding to the highest displacement toward downstream and upstream directions, respectively. The assigned load combinations corresponding to these two dates and the loads involved in the dynamic analysis are depicted in Table 5.

As designated in Table 5, the dynamic analyses are executed under the earthquake level of MCE. Actually experiencing such an excitation (June, 1990 earthquake), SefidRud dam is analyzed under ABBAR earthquake records in three directions (see Fig. 6), with PGAs of 0.55 g, 0.49 g and 0.52 g in US/DS (Upstream-Downstream), cross stream and vertical directions,

respectively. These earthquake records are applied to the foundation far end and bottom nodes, simultaneously.

Furthermore, the dynamic analysis necessitates the amplification of some parameters to account the rapid loading impact. The required amplifying factors are listed in Table 6. The other parameters not mentioned in Table 6 are presumed to have a unit amplifying factor. And just as importantly is the dissipative mechanism of the materials for such a seismic model which contains the Reighly damping based on 10% damping ratio and the structure's first and second vibration modes in direction of the river flow based on comment in USACE manual (U.S. Army Corps of Engineers 2007).

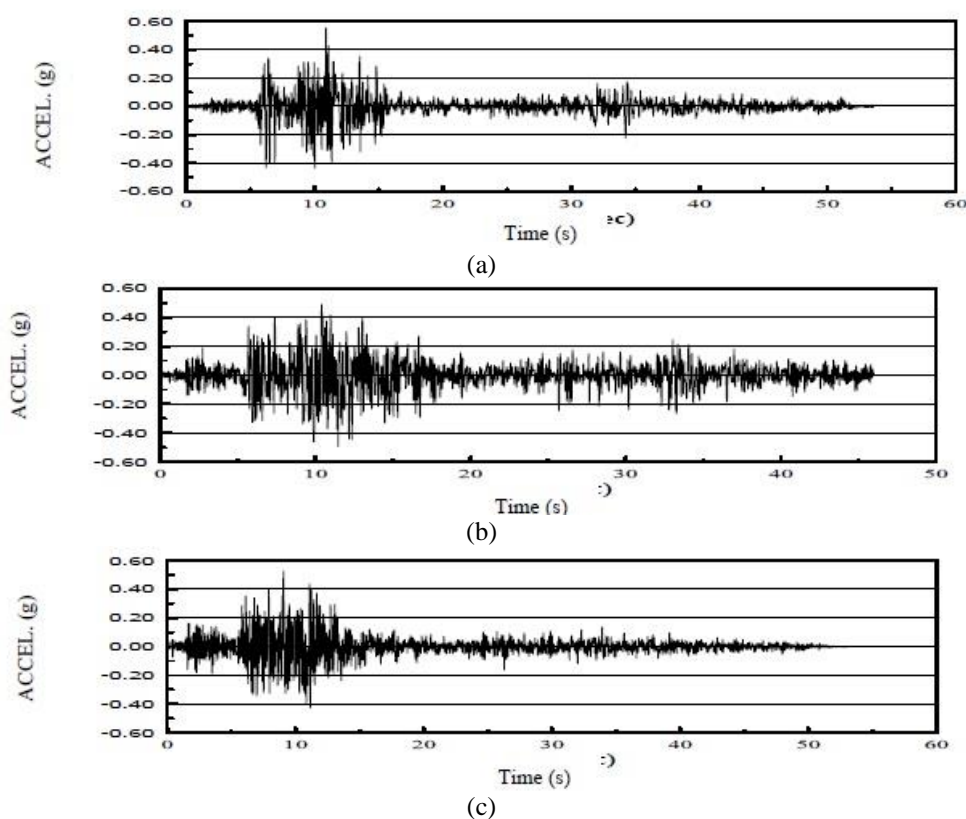


Fig. 6 ABBAR earthquake records in (a) US/DS, (b) cross stream, and (c) vertical direction

Table 5 Load combination and its components in dynamic analysis

Load combination	Loading description	Considerations
First	Weight + temperature on date April, 4, 1999 + corresponding reservoir level (maximum)+ earthquake MCE	Operating condition date April, 4, 1999
Second	Weight + temperature on date Aug, 8, 1999 + corresponding reservoir level (minimum)+ earthquake MCE	Operating condition date Aug, 8, 1999

Table 6 The amplifying factors for dynamic analysis

Parameter	Amplifying factors	Ultimate value
Concrete elasticity modulus	1.25	23.75 GPa
Compressive strength	1.3	21.8 MPa
Concrete tensile strength	1.5	3.2 MPa
Concrete apparent tensile strength	1.5	4.35 MPa

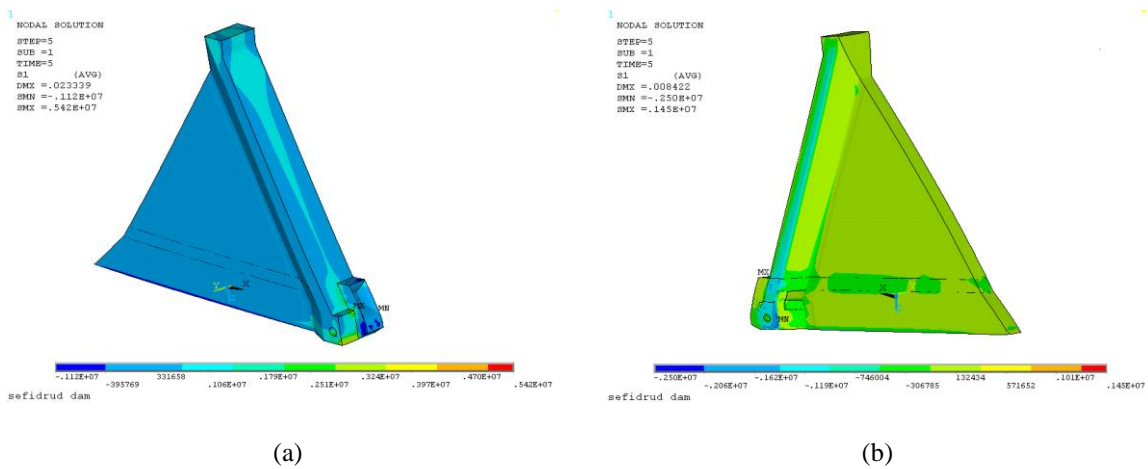


Fig. 7 Maximum static principal stress distribution on the dam body in operating conditions of (a) April, 4, 1999, and (b) Aug, 8, 1999

Considering the material properties and the boundary conditions variations originated from various types of analysis (static and dynamic), the sequence of the mentioned loads assignment must be implemented with some caution. At the first step, only the dam weight with the static properties is imposed. Remaining the static properties, the assigned load shifts to the thermal load corresponding to the empty reservoir and then, under the same conditions, the hydrostatic load and the uplift pressure act to the model. The uplift pressure distribution is assumed to be linear decreasing from the head of the reservoir at the heel to its half aligned with the bottom gallery (after grout curtain) and then, decreasing to the head of the downstream water at the toe. This pressure is fluctuated in accordance with the head of the reservoir. The fourth step is devoted to the thermal load assignment corresponding to the water levels designated in Table 5 by imposing creep affection (Table 4). It is worth mentioning that effect of the block side displacement is ignored (USCOLD 1992) during all stages of conducted analyses. Clearly, this limitation on the lateral displacement is applied along the head of block and the remaining parts like the buttress is free for lateral vibration/displacement. The recorded performance of the dam body during Manjil 1990 earthquake and investigations reported like Ghaemmaghmi and Ghaemian (2008) and Ghaemmaghmi and Ghaemian (2010) confirm this assumption (there is not any crack showing the lateral vibration or displacement within the head in block No. 18). Earthquake analysis after the pre-earthquake static conditions ends the loading sequence.

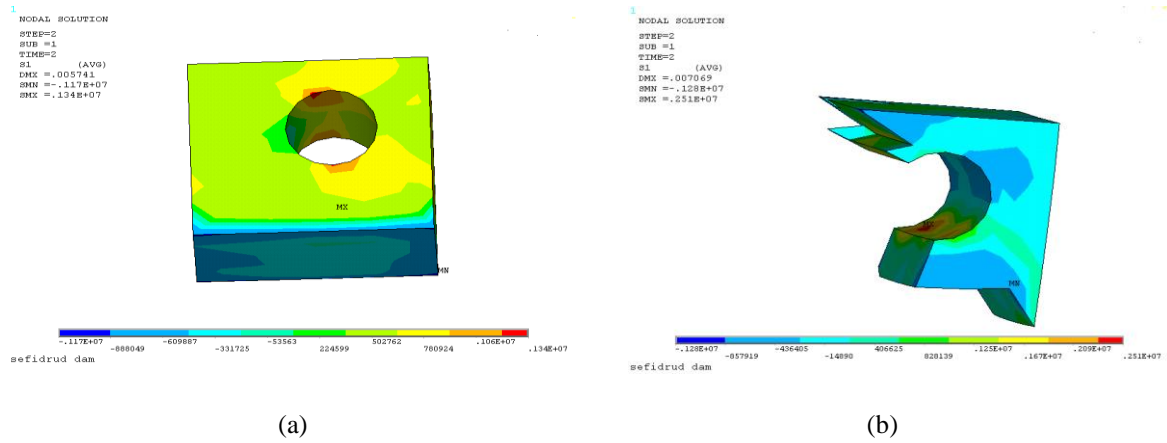


Fig. 8 Maximum static principal stress distribution in the gallery of block No. 18 in empty reservoir condition and thermal circumstance of (a) April, 4, 1999, and (b) Aug, 8, 1999

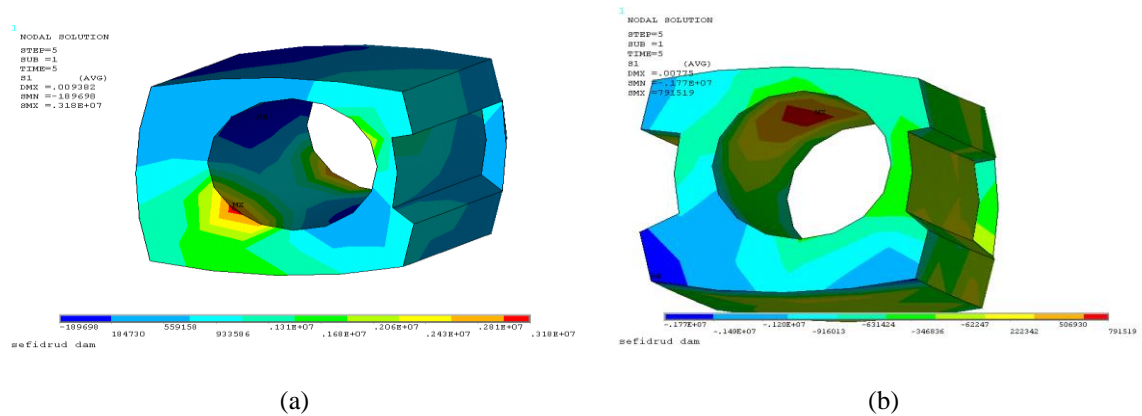


Fig. 9 Maximum static principal stress distribution in the gallery of block No. 18 in operating conditions of (a) April, 4, 1999, and (b) Aug, 8, 1999

To detect the whereabouts of the probable failure and to facilitate the estimation of the fractured regions a static analysis precedes the linear dynamic one. In Fig. 7 the result of such an analysis is demonstrated in operating conditions.

As it is observed, the foundation gallery zone is exposed to the highest static tensile stress remarkably differing from the other regions of the dam body. Accordingly, this zone experiences static tensile stresses of 5.42MPa and 1.45MPa on April, 4, 1999 and Aug, 8, 1999, respectively. Although this excessive stress stem from the stress concentration, exceeding tensile strength (2.15MPa in Table 4) in the case of maximum water level (April) necessitates a more accurate investigation of block No. 18 gallery. This requirement is fulfilled in Figs. 8 and 9 which yield a more precise comprehension of crack initiation and its propagation in the block gallery.

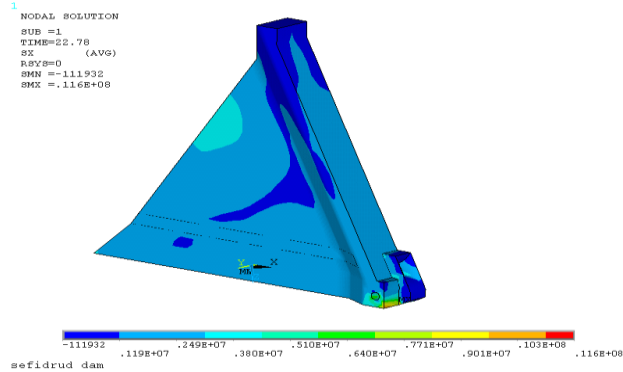


Fig. 10 The maximum principal stress envelope for the first load combination

A closer inspection of block No.18 foundation gallery under the empty reservoir condition and thermal loads, simulating the construction phase conditions, reveals the probable initiation of the crack because of the hot climate induced thermal load (Fig. 8(b)) on the gallery ceiling and the internal wall where a maximum tensile stress of 2.51MPa is observed which exceeds the concrete tensile strength (2.15MPa). The maximum tensile stress level for the cold climate (1.34MPa) refuses to have the same results (Fig. 8(a)). The tensile stress in the gallery even grows higher under the static load by increasing the reservoir level until it reaches the magnitude of 3.18MPa in the operating conditions of maximum water level (Fig. 9(a)) and causes further expansion of the crack. These findings coincide with the previous reports and observations including the seepage flow rate from the cracks in operation phase in various climate condition (resembling the analysis controlling dates) reducing from 1.83l/s on March, 26, 1999 (cold condition) to 0.16l/s on July, 26, 1999 (hot condition) where the maximum tensile stress falls below the concrete tensile strength (Fig. 9(b)). Despite the crack initiation and expansion in construction and operation phases, the stability of the dam under the static loads can be claimed safe regarding the minor expansion of high tensile stresses in depth and width of the gallery.

Recognizing the potential failure regions, a dynamic analysis is required to assess the stability of the block under more severe seismic loads for the two load combinations designated in Table 5. Fig. 10 reveals the maximum tensile stress envelope for the earthquake duration of 25s based on the case of maximum water level (the first load combination).

Accordingly, an intense maximum tensile stress of 11.6MPa is observed in a very small area on the dam heel which can be ignored because of the minor spread of such an area, therefore, it can be asserted that the block No.18 safety will not be compromised by that zone. It is worth mentioning that the high stresses at the toe of the concrete dams are common and are eliminated in the real condition because of the joint opening between the dam body and the foundation rock. In addition, considering the reinforcement embedded in the gallery surrounding mass concrete, having high stresses within this region just lead to some leakage and we have no safety concern in general. But what about the other regions on the dam body? For now, let's put aside the gallery and investigate the other areas as shown in Fig. 11.

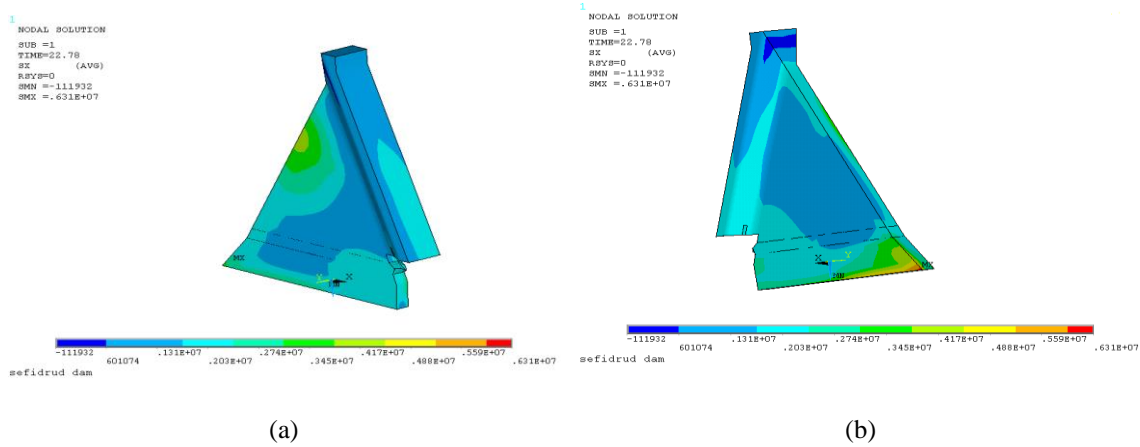


Fig. 11 The maximum principal stress envelope for the first load combination in the absence of the gallery and the outlet

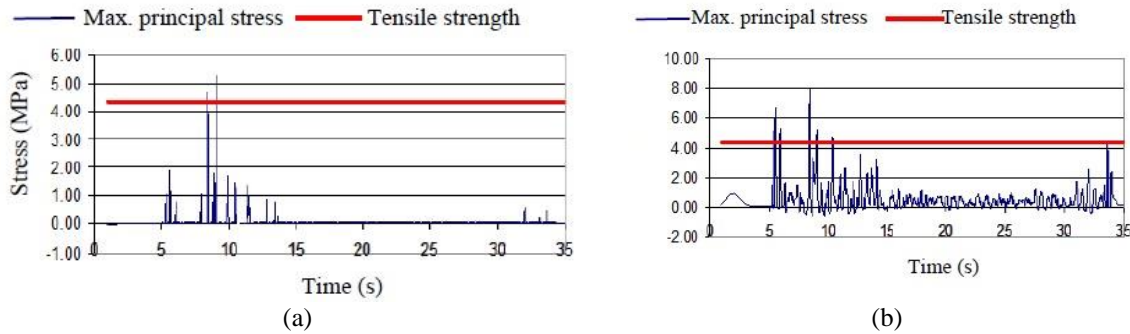


Fig. 12 The upper limit of the tensile stress and the variation of the Maximum principal stress at (a) the middle portion of the downstream face, and (b) the dam toe, for the first dynamic load combination

It can be observed that the relatively high tensile stresses of 5MPa and 6.6MPa emerge on the middle portion of the buttress downstream face (Fig. 11(a)) and the dam heel (Fig. 11(b)), respectively. In regard to their rather excessive magnitudes in comparison with the concrete dynamic tensile strength, 4.35MPa, and the vast expansion of such areas, an estimation of the associated damage level is inevitable. Such a task is accomplished via the concrete gravity dam Demand-Capacity Ratio (DCR) curves of the suspected spots, Fig. 12.

Accordingly, the number of the stress limit passing and the cumulative inelastic duration of both downstream face middle portion (Fig. 12(a)) and the dam toe (Fig. 12(b)) lie in an acceptable damage range based on the concrete gravity dams performance curve determined in USACE manual (U.S. Army Corps of Engineers 2003) and there is no threat form these zone side for cracking severity. Consequently, the only factor left threatening the total safety of the block is the expansion of the existing crack in gallery resulting from the seismic loads. Fig. 13 depicts the maximum principal stress distribution in gallery region and its time history under the first load combination.

Regions of severe tensile stress with a significant depth form on the vast width of the gallery internal wall (Fig. 13(a)). Moreover, not only the intense magnitude and the wide expansion of the tensile stress, but also the associated cumulative inelastic duration goes over the permissible range (Fig. 13(b)) and result in the creation of new cracks and propagation of the existing ones. The growth of the seepage after the Roudbar-Manjil earthquake proves the idea. But, does it jeopardize the general dam safety? A trustworthy response to this essential question leads us to the nonlinear analysis of the challenging region, the block gallery. But before that, let's proceed the linear dynamic analysis for the second load combination. Fig. 14 illustrates the associated results.

The middle portion of the downstream face within the buttress (Fig. 14(a)) and the dam toe (Fig. 14(b)) are again exposed to the intense but not destructive tensile stresses because of the inelastic duration and the damage level minority (see Fig. 15).

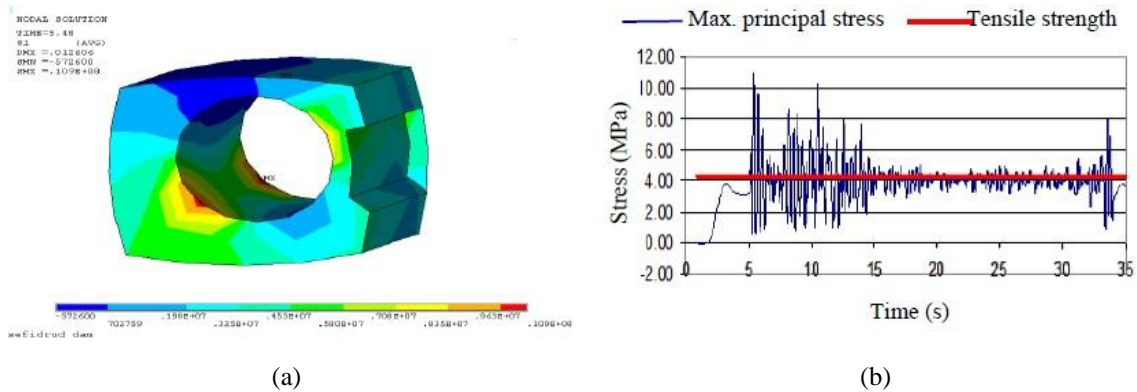


Fig. 13 (a) The maximum principal stress distribution contour, and (b) the maximum principal stress time history of the highest stress spot for the first load combination

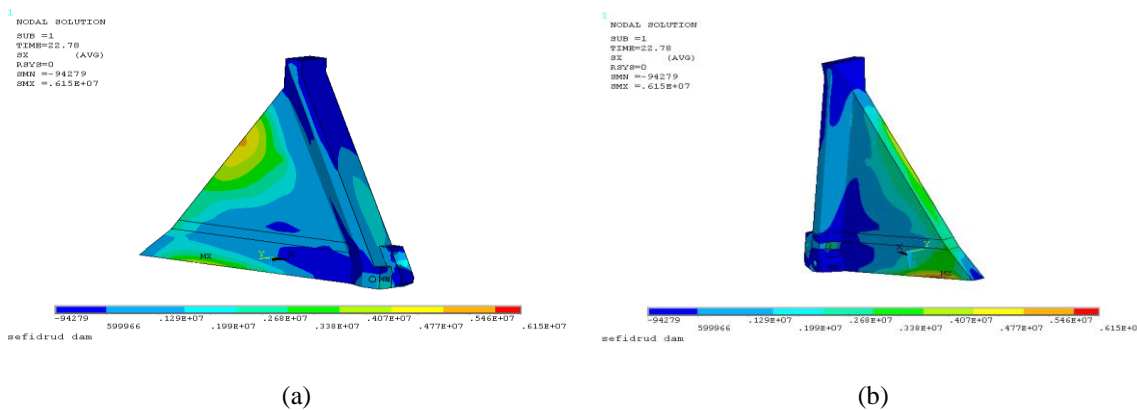


Fig. 14 The maximum principal stress envelope for the second load combination

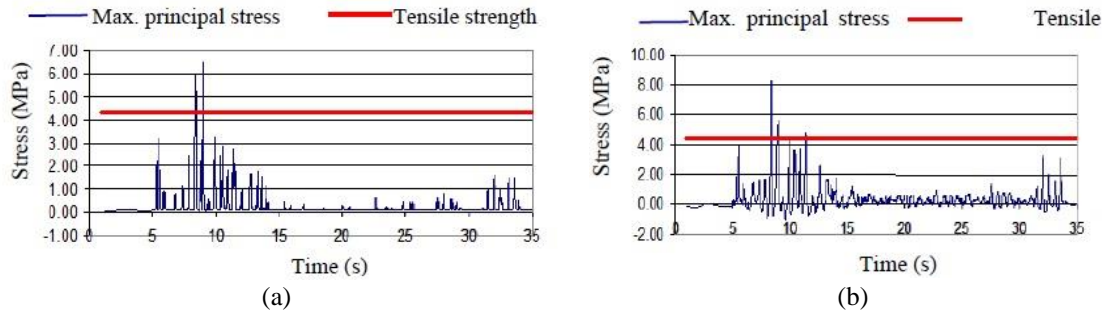


Fig. 15 The upper limit of the tensile stress and the variation of the Maximum principal stress at (a) the middle portion of the downstream face, and (b) the dam toe, for the second dynamic load combination

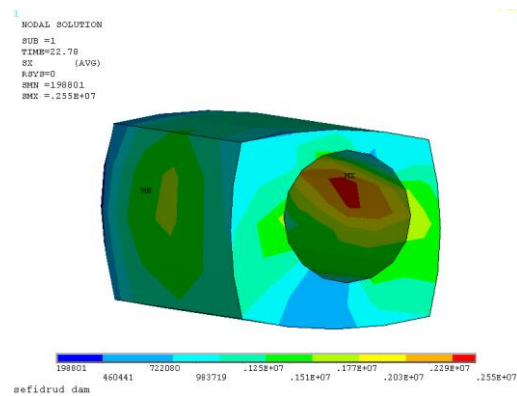


Fig. 16 The maximum principal stress envelope in gallery for the second load combination

For the problematic case of the block gallery, the concrete tensile strength is not even met under the second load combination and a maximum tensile stress of 2.6MPa appears on the gallery internal wall (see Fig. 16).

So, under the minimum reservoir level condition, the dam total stability is assessed safe and no specific deflection develops. As a consequence, the nonlinear analysis for the maximum reservoir level condition (the first load combination) seems to be mandatory.

5. Nonlinear analysis

Considering the results from the static and linear dynamic analyses, a nonlinear analysis under the seismic loads seems to be a wise choice to assess the deflections level and the associated expansion especially in the foundation gallery and in bigger picture, to estimate the general stability of the dam. In every steps of the loading sequence in the nonlinear model, the most critical conditions are taken into the account. For instance, for the loads associated with the full

reservoir, the conditions on April, 4, 1999 is applied while the loads involving the empty reservoir (construction phase) deals with the conditions on Aug, 8, 1999. Regarding the loading sequence in the linear dynamic analysis, there is an extra step at the end of the loading which includes 4-meter gradual reduction of the reservoir water level to simulate the post-earthquake water release from the reservoir. It is noteworthy that the *Smearred crack* model is applied in the conducted nonlinear analysis (see Appendix,(ANSYS)). Accordingly, Fig. 17 illustrates the crack expansion process in block No.18 gallery internal wall and the culvert box during the whole nonlinear analysis.

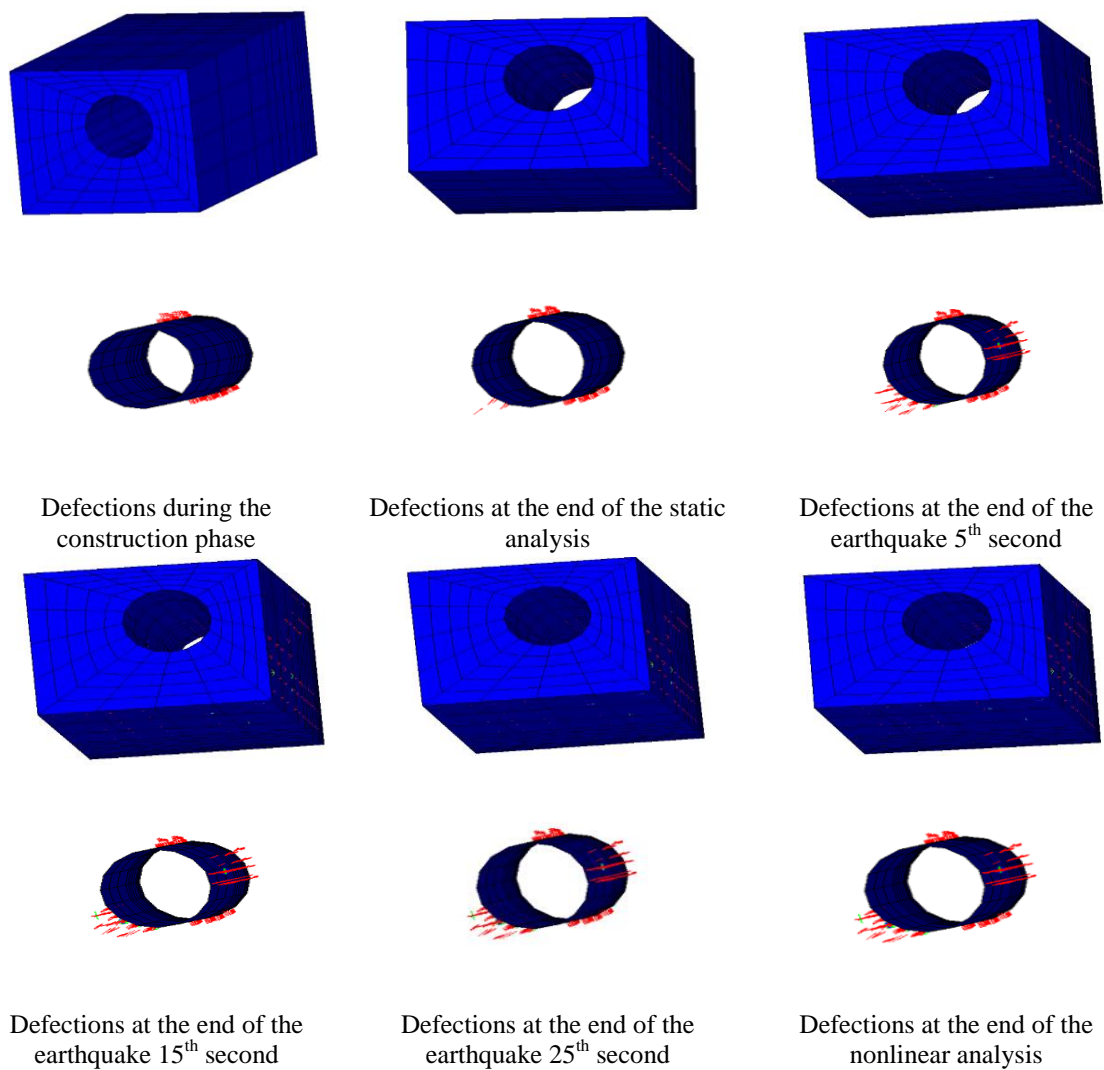


Fig. 17 Crack expansion process in the gallery box and its internal wall during the nonlinear analysis

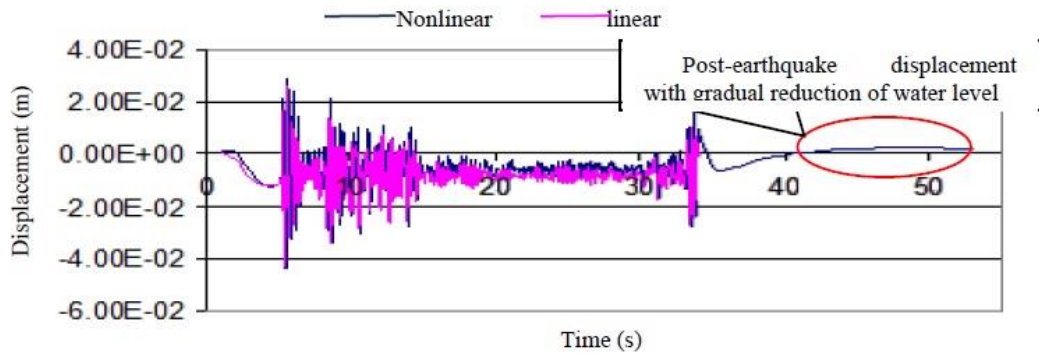


Fig. 18 The crest displacement time history in linear and nonlinear analysis (+ toward upstream and – toward downstream)

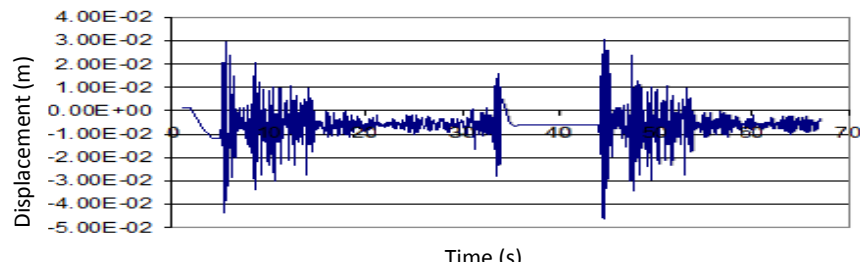


Fig. 19 The dam crest displacement time history in nonlinear analysis of the two successive earthquake (+toward the upstream, and – toward the downstream)

In the above shown pictures, the red marks describe the deflection zones. Accordingly, the cracks initiate at the construction phase from the internal wall and expand in width and depth during the static loading and the first 15s of the earthquake, but after that the expansion halts and no further fractures is generated. The crack expansion termination guarantees the general stability of the dam body. Fig. 18 seals this claim by comparing the crest displacement time history from the linear and nonlinear analyses.

As can be seen in Fig. 18, the crest displacement records in both linear and nonlinear analyses remarkably coincide and there is no sign of an abrupt jump and termination of the nonlinear records which proves the numerical and structural stability of the dam. In addition, at the end of the nonlinear analysis one can recognize the crest displacement toward the upstream with a moderate slope which is proportional to the reservoir water level gradual decline and demonstrating the nonentity of the general dam failure. According to the nonlinear analysis results, the satisfaction of the total stability of the dam is due to the permissible fracture expansion, particularly in block No. 18 gallery. But does it mean that the dam can withstand an intense future earthquake regarding the current damages? To check that, all it takes is applying another earthquake back-to-back with the first one and running a new nonlinear analysis. For this purpose, 23s of the first earthquake record including the peak acceleration is imposed to the system as the

upcoming earthquake instead of the water level gradual reduction step in loading sequence of the primary nonlinear analysis. Fig. 19 represents the crest displacement time history of such an analysis.

The second earthquake launches at 44th second. According to Fig. 19, despite a slight difference in system responses of the first and the second earthquakes (in favor of the second one), the trend and the peak values in both excitations acceptably match (-43.8 mm and +29.5 mm from the first earthquake and -46.4 mm and +30.5 mm caused by the second one) indicating the crack minor effect in the gallery as the riskiest zone and consequently the system stability even under another severe MCE record. The fracture expansion process inside the gallery demonstrate this notion schematically in Fig. 20.

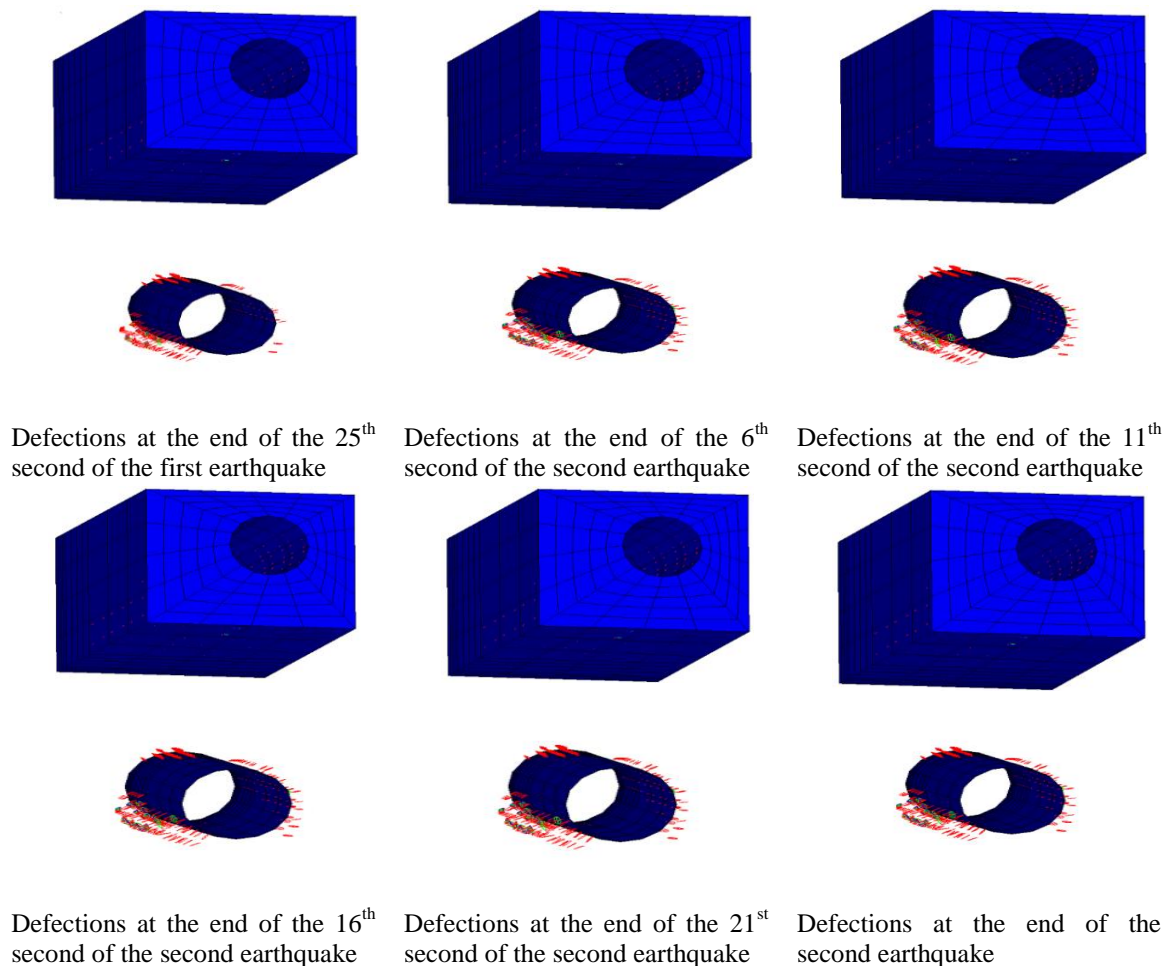


Fig. 20 Crack expansion process in the gallery box and its internal wall during the nonlinear analysis of the two successive earthquakes

Accordingly, a slight growth is observed in crack extension under the second earthquake comparing with the first one. These defections mainly spread in vicinity of the existing cracks or in the intense tensile stress areas and rather toward upstream. In spite of the deflection anticipation in the dam body and the crack opening in the dam gallery leading to the seepage growth, the general stability of the SefidRud dam will not encounter with any threat because of the crack expansion suspension even in the case of a recurring intensive earthquake (similar to ABBAR earthquake).

5. Discussion

Clearly, the conducted study has several shortcomings. In the smeared crack approach utilized for nonlinear analyses, the potential area for cracking and leakage can be predicted. However, there is not any accurate results on residual displacements. Then, a complementary study incorporating a discrete crack approach seems to be required. In addition, the foundation is assumed to be massless. Massless foundation leads to more conservative results. The joint between the dam body and the foundation just beneath that is neglected. This assumption leads to limited stress concentration at the heel which is not realistic.

Assuming a high damping ratio may lead to un-conservative results. Estimating a reasonable value for damping ratio which is a function of stress amplitude and material properties is the subject of the next studies by the authors.

At last, the uplift pressure is assumed to be in accordance with the reservoir water level during the first and second earthquakes and so, there is not any uplift increase after the earthquake occurrence.

6. Conclusions

In present study, a dynamic investigation of SefidRud dam block No.18 has been represented to examine its seismic stability regarding the existence of cracks in the foundation gallery. For this purpose, a three dimensional finite element model was characterized consisting the dam body, the foundation and its gallery, and the reservoir. The analysis parameters were designated through the thermal and structural calibrations with the thermometers and the direct pendulum installed inside the dam body. The seismic analyses under the three components of the MCE records (ABBAR earthquake) were focused on the two specific dates of April, 4, 1999 and Aug, 8, 1999 corresponding to the highest displacement toward the upstream and downstream, respectively. Based on the primary thermal and static analyses, because of the crack initiation under the thermal load in the construction phase, the foundation gallery turned out to be the most probable zone to menace the block No.18 and the dam general safety. The results of the linear dynamic analysis verified this claim where under the seismic loads the mentioned fractures started propagating and in consequence, the seepage increased. The available reports measuring the seepage from the cracks had demonstrated that the seepage flow rate on March, 26, 1999 (similar condition with April, 4, 1999) reached 1.83l/s while in July, 26, 1999 it reduced to 0.16l/s (in condition resembling Aug, 8, 1999). Beside the crack seepage growth, according to the gravity dam performance curve, the deflection expansion necessitated a nonlinear analysis of block No.18 for a trustworthy estimation of damage level and the total dam safety. As a result, through a *smeared crack* model, it was observed that the crack expansion halted from the 15th second of the

earthquake and reached a steady state. Besides, there was no abrupt jump or termination in the crest displacement time history and even under another severe upcoming earthquake the total dam safety did not confront serious threat. Nevertheless, in case of an intensive future earthquake, particularly for the full reservoir, regarding the gallery crack growth and the existing fracture development, the following steps should be carried out:

- The primary reduction of the reservoir water level won't be required according to the nonlinear results.
- During the first 48 hours after the earthquake, according to the visual inspection of the damage level and extent and in regard to the post-earthquake seepage flow rate and the uplift pressure, the appropriate decision of water level reduction should be made.
- During the first two weeks or the first month after the earthquake, based on the monitoring instruments records and more accurate inspections, probable rehabilitation procedures or further water level reduction should be accomplished.

However, the conducted study has shortcoming as mentioned in previously. One of the major shortcomings is the reasonable value of damping ratio and estimating the residual displacement utilizing a comprehensive discrete crack modeling.

References

- Ahmadi, M. and Khoshrang, G. (1992), "SefidRud dam's dynamic response to the large near-field earthquake of June 1990", *Dam Eng.*, **3**, 85-115.
- Ahmadi, M., Khoshrang, G., Mokhtarzadeh, A., and Jalalzadeh, A. (1992), "Behaviour of a large concrete dam due to an actual maximum credible earthquake", *Proceedings of the Earthquake Engineering, Tenth World Conference, Balkema, Rotterdam*.
- ANSYS, Inc. Theory Reference Manual.
- Arcangeli, E. and Ciabbari, P. (1994), "Menjil dam rehabilitation by resin grouting and high capacity anchors", *Int. Water power Dam Constr.*, **46**, 19-25.
- Bofang, Z. (1997), "Prediction of water temperature in deep reservoir", *Dam Eng.*, **8**, 13-25.
- FERC (1999), Engineering Guidelines for the Evaluation of Hydropower Projects, Federal Energy Regulatory Commission, Division of Dam Safety and Inspections, Washington, DC 20426.
- Ghaemian, M. (1996), "Seismic response of a retrofitted concrete buttress dam", *Proc., 11th WCEE, Acapulco, Mexico*.
- Ghaemian, M. and Ghobarah, A. (1997), "Seismic response of the Sefidrud concrete buttress dam", *Eur. Earthq. Eng.*, **11**, 7-16.
- Ghaemian, M., and Ghobarah, A. (1998), "Staggered solution schemes for dam-reservoir interaction", *J. Fluids Struct.*, **12**, 933-948.
- Ghaemian, M. and Ghobarah, A. (1999), "Nonlinear seismic response of concrete gravity dams with dam-reservoir interaction", *Eng. Struct.*, **21**, 306-315.
- Ghaemmaghami, A. and Ghaemian, M. (2008), "Experimental seismic investigation of Sefid-rud concrete buttress dam model on shaking table", *Earthq.Eng. Struct. D.*, **37**, 809-823.
- Ghaemmaghami, A. and Ghaemian, M. (2010), "Shaking table test on small-scale retrofitted model of Sefid-rud concrete buttress dam", *Earthq.Eng. Struct. D.*, **39**, 109-118.
- Ilinca, C., Vărvorea, R. and Popovici, A. (2014), "Influence of dynamic analysis methods on seismic response of a buttress dam", *Math. Model. Civil Eng.*, **10**, 12-26.
- Shen, C.K., *et al.* (1974), "Earthquakes induced by reservoir impounding and their effect on the Hsinfengkiang Dam", *Scientia Sinica*, **17**, 239-272.

- USACE EM 1110-2-6051 (2003), Time-History Dynamic Analysis of Concrete Hydraulic Structures. Chapter 4: Structural Performance and Damage Criteria, U.S. Army Corps of Engineers; Washington, DC, USA.
- USACE EM 1110-2-6053 (2007), Earthquake Design and Evaluation of Concrete Hydraulic Structures, U.S. Army Corps of Engineers; Washington, DC, USA.
- USCOLD. (1992), Observed Performance of Dams During Earthquakes, USCOLD Committee on Earthquakes.
- Yekom Consulting Engineers (2007), “Rehabilitation project of Sefid Roud, Static analysis of butress number 18”, Yekom Consulting Engineers,.

JK

Appendix

The smeared crack model is classified as a continuum model in fracture analysis of concrete dams. In this model, in contrast with the discrete ones, the mesh remains intact and instead, the material constitutive relation is updated during the crack propagation with the reference axis aligned with the fracture direction.

The concrete is assumed linear and isotropic initially; so, its pre-crack constitutive relation is as follows

$$[D_{linear}] = \frac{E}{(1+\nu)(1-2\nu)} \begin{bmatrix} (1-\nu) & \nu & \nu & 0 & 0 & 0 \\ \nu & (1-\nu) & \nu & 0 & 0 & 0 \\ \nu & \nu & (1-\nu) & 0 & 0 & 0 \\ 0 & 0 & 0 & \frac{1-2\nu}{2} & 0 & 0 \\ 0 & 0 & 0 & 0 & \frac{1-2\nu}{2} & 0 \\ 0 & 0 & 0 & 0 & 0 & \frac{1-2\nu}{2} \end{bmatrix} \quad (1)$$

where E and ν are the concrete isotropic Young's modulus and Poisson's ratio, respectively. When the crack initiates, this constitutive relation is modified by defining a weak plane normal to the crack direction not bearing the tensile stresses and applying the shear transfer coefficient in the cracked plane. The updated constitutive relation based on the crack directions can be classified as follows:

I) One-directional open crack

$$[D_{cracked}^{open}] = \frac{E}{1+\nu} \begin{bmatrix} \frac{E^s(1+\nu)}{E} & 0 & 0 & 0 & 0 & 0 \\ 0 & \frac{1}{1-\nu} & \frac{\nu}{1-\nu} & 0 & 0 & 0 \\ 0 & \frac{\nu}{1-\nu} & \frac{1}{1-\nu} & 0 & 0 & 0 \\ 0 & 0 & 0 & \frac{\beta_{open}}{2} & 0 & 0 \\ 0 & 0 & 0 & 0 & \frac{1}{2} & 0 \\ 0 & 0 & 0 & 0 & 0 & \frac{\beta_{open}}{2} \end{bmatrix} \quad (2)$$

In which E_s represents the secant modulus of elasticity and β_{open} demonstrates the shear strength reduction across the cracked face in open cracks.

II) One-directional closed crack

$$[D_{cracked}^{closed}] = \frac{E}{(1+\nu)(1-2\nu)} \begin{bmatrix} (1-\nu) & \nu & \nu & 0 & 0 & 0 \\ \nu & (1-\nu) & \nu & 0 & 0 & 0 \\ \nu & \nu & (1-\nu) & 0 & 0 & 0 \\ 0 & 0 & 0 & \frac{\beta_{close}(1-2\nu)}{2} & 0 & 0 \\ 0 & 0 & 0 & 0 & \frac{1-2\nu}{2} & 0 \\ 0 & 0 & 0 & 0 & 0 & \frac{\beta_{close}(1-2\nu)}{2} \end{bmatrix} \quad (3)$$

where β_{close} is closed shear transfer coefficient varying from 0.0 to 1.0, with 0.0 representing a smooth crack (complete loss of shear transfer) and 1.0 indicating a rough crack (no loss of shear transfer).

III) Two-directional open crack

$$[D_{cracked}^{open}] = E \begin{bmatrix} \frac{E^s}{E} & 0 & 0 & 0 & 0 & 0 \\ 0 & \frac{E^s}{E} & 0 & 0 & 0 & 0 \\ 0 & 0 & 1 & 0 & 0 & 0 \\ 0 & 0 & 0 & \frac{\beta_{open}}{2(1+\nu)} & 0 & 0 \\ 0 & 0 & 0 & 0 & \frac{\beta_{open}}{1(1+\nu)} & 0 \\ 0 & 0 & 0 & 0 & 0 & \frac{\beta_{open}}{2(1+\nu)} \end{bmatrix} \quad (4)$$

IV) Two-directional closed crack

$$[D_{cracked}^{closed}] = \frac{E}{(1+\nu)(1-2\nu)} \begin{bmatrix} (1-\nu) & \nu & \nu & 0 & 0 & 0 \\ \nu & (1-\nu) & \nu & 0 & 0 & 0 \\ \nu & \nu & (1-\nu) & 0 & 0 & 0 \\ 0 & 0 & 0 & \frac{\beta_{close}(1-2\nu)}{2} & 0 & 0 \\ 0 & 0 & 0 & 0 & \frac{(1-2\nu)}{2} & 0 \\ 0 & 0 & 0 & 0 & 0 & \frac{\beta_{close}(1-2\nu)}{2} \end{bmatrix} \quad (5)$$

V) Three-directional open crack

$$[D_{cracked}^{open}] = E \begin{bmatrix} \frac{E^s}{E} & 0 & 0 & 0 & 0 & 0 \\ 0 & \frac{E^s}{E} & 0 & 0 & 0 & 0 \\ 0 & 0 & 1 & 0 & 0 & 0 \\ 0 & 0 & 0 & \frac{\beta_{open}}{2(1+\nu)} & 0 & 0 \\ 0 & 0 & 0 & 0 & \frac{\beta_{open}}{2(1+\nu)} & 0 \\ 0 & 0 & 0 & 0 & 0 & \frac{\beta_{open}}{2(1+\nu)} \end{bmatrix} \quad (6)$$

VI) Three-directional closed crack: The same as case IV.